

Determining Localized Necking in Polycrystalline Sheet Metals Using the Bifurcation Phenomenon in Strain Evolution

Ji He ^{1,2,*} and Yishuang Feng ²

¹ State Key Laboratory of Mechanical System and Vibration, Shanghai Jiao Tong University, Shanghai 200240, China

² Shanghai Key Laboratory of Digital Manufacture for Thin-Walled Structures, Shanghai Jiao Tong University, Shanghai 200240, China

* Correspondence: benbenhj@sjtu.edu.cn

Abstract: The forming limit is an important failure criterion for polycrystalline sheet metals when approving the forming process. Recent developments in strain measurement technology, e.g., digital image correlation (DIC), enable the strain evolution to be captured continuously and accurately. This new technology would improve the forming limit measurements if the onset of the necking detection method was developed accordingly. This paper proposes a new method based on the bifurcation phenomenon in strain evolution to detect the onset of localized necking through DIC measurements. This detection method was inspired by a physical understanding and experimental observations of the necking phenomenon. The method eliminates the derivative calculation from the traditional method, while it can directly determine the onset of localized necking through strain evolution curves. The robustness and accuracy of the method are also investigated through experiments. Imperfection and non-defect analyses, based on non-associated and associated flow rules, were utilized and compared to the determined results. The detection method provides satisfactory forming limit results and can be used as an alternative method to determine the forming limit diagram (FLD).

Keywords: localized necking; forming limits; bifurcation analysis; digital image correlation



Citation: He, J.; Feng, Y. Determining Localized Necking in Polycrystalline Sheet Metals Using the Bifurcation Phenomenon in Strain Evolution. *Crystals* **2023**, *13*, 272. <https://doi.org/10.3390/cryst13020272>

Academic Editor: Li-Wei Tseng

Received: 6 December 2022

Revised: 30 January 2023

Accepted: 2 February 2023

Published: 4 February 2023



Copyright: © 2023 by the authors. Licensee MDPI, Basel, Switzerland. This article is an open access article distributed under the terms and conditions of the Creative Commons Attribution (CC BY) license (<https://creativecommons.org/licenses/by/4.0/>).

1. Introduction

A forming limit diagram (FLD) is a criterion for judging whether the obtained sheet metal component is safe or necked. The accuracy of its representation directly affects decisions to approve the forming process. Localized instability analysis, proposed by Hill [1] in 1952, laid the theoretical foundation for the prediction of the tensile instability of sheet metals. In 1965, Keeler [2] proposed the concept of forming limit diagrams in an SAE report, which was further supplemented by Goodwin [3] in 1968. When localized instability (or the bifurcation phenomenon) occurs, a groove appears on the surface, and the crack expands rapidly, causing the failure of the sheet [4,5]. The bifurcation phenomenon of the sheet metal means a localized deformation in a narrow band, while the deformation remains homogeneous elsewhere [6,7]. Therefore, the localized instability stage (also known as localized necking) is generally considered as the maximum allowable deformation of the sheet, and the strain at the beginning of the localized instability stage is used as the limit strain for judging whether the sheet has failed [8].

The most commonly used test method for establishing a forming limit diagram at present is the Nakazima hemispherical bulging test [9] or the modified flat punch bulging test by Marciniak et al. [10]. The acquisition of a reliable limit strain is one of the most concerning issues in the study of forming limits. A new development in strain measuring, referred as digital image correlation (DIC), allows the strain evolution to be recorded continuously and accurately for the entire experimental procedure. This certainly provides the possibility of obtaining more accurate necking limits in the strain space. However, the core challenge is to propose a method to determine the onset of localized necking.

DIC technology tracks the speckle movement on the top surface of the specimen and further calculates the strain field according to time. In general, two essential points should be determined through the experimental procedure: (i) the instant of localized necking to indicate the timing and (ii) the location of localized necking to indicate the limit strain.

One popular method is the so-called space-dependent method, where the major strain of the points on the cross section perpendicular to the crack growth direction after fracture is used to fit an inverse parabola, and the limit strain is determined by the vertex of the inverse parabola [9]. Generally, the space-dependent method only considers a certain deformation state of the specimen and does not pay attention to the deformation history. The emergence and development of digital image correlation technology have led to the development of analysis and measurement methods based on strain history.

Huang et al. [11] obtained the relationship between the second derivative of strain and time. They believed that the increase in the second derivative near the fracture indicates the beginning of localized necking, and the limit strain is determined correspondingly. Merklein et al. [12] performed regression analysis on the major strain rate in the center of the necking region. The extreme point of specific parameters obtained from the regression analysis was considered to be the start of localized necking. Hotz et al. [13] used the first derivative of the thickness strain versus the punch position to determine the onset of localized necking and put forward constructive comments on the calculation of the derivative. Martínez-Donaire et al. [14] suggested that the major strain rate at the boundary point of the instability zone first increases and then decreases with the deformation of the sheet. The extreme point of the major strain rate corresponds to the onset of localized necking. Min et al. [15] compared the forming limit diagrams of several different sheet metals. It was found that the circular mesh strain analysis technique always overestimates the limit major strain of the material, but the method of the ISO standard [9] underestimates the limit strain. Therefore, they proposed that if the limit strain is to be more accurately obtained, it is necessary to consider the spatial and time factors in order to capture the subtle changes in the sample when localized necking occurs, due to the fact that localized necking is an unstable physical process with both spatial and temporal characteristics.

From the perspective of physical understanding, parameters related to the thickness strain (ϵ_3) may be more worthy of attention. The physical interpretation of localized necking is the sudden thinning of the sheet in the thickness direction (or bifurcation phenomenon); thus, relevant parameters of ϵ_3 directly reflect the deformation of the polycrystalline sheet metal along the thickness direction. Wang et al. [16] selected two points on the cross-section of their sample perpendicular to the crack growth direction. One point was selected at the center of the crack, and the other was away from the center. The difference between the heights of the two points was recorded. The first derivative of the height difference (ΔZ) could then be calculated, and it was considered that the sudden increase in the first derivative represented the onset of localized necking. Di et al. [17] used the local surface curvature of the sample to determine the onset of localized necking. Min et al. [18] proposed a two-dimensional curvature criterion based on the ordinate value of the cross-section of the crack growth direction.

In many deterministic approaches to localized necking, the first derivation is necessary to capture the timing and the strain limit. From a practical point of view, if the DIC signal is not prepared properly, the derivation will be too noisy to use. Thus, such an approach requires extensive operator experience and could be tedious and labor-intensive. This paper aims to develop an approach to determine the onset of localized necking in polycrystalline sheet metals, while eliminating the derivative calculation. The physical interpretation of localized necking under uniaxial tension is also utilized to shed light on this necking deterministic approach. The experimental results and theoretical prediction are compared to help us achieve an in-depth understanding of the correlation between the bifurcation in strain evolution and localized necking.

To achieve this purpose, we (i) first introduce the tested materials and the experimental procedures used in this study; (ii) investigate the bifurcation phenomenon in the strain

evolution under uniaxial tension tests; (iii) provide the detailed detection procedure based on the bifurcation phenomenon to capture the limit strains; and (iv) compare and analyze the final forming limits to illustrate the effectiveness of the proposed method.

2. Technical Details and Methods

2.1. Material Characterization and Properties

High-strength steel sheets with an approximate 600 MPa yield stress grade and low-carbon steel sheets were employed in this study. The high-strength steel sheets were tested using the standard Nakazima tests [9]. The low-carbon steel sheets were tested using home-made mini-Nakazima tests since the strength of this material is within the output load range of the universal testing machine.

To obtain the mechanical properties of the material under simple tension loading, the uniaxial tension test was conducted on 0.7 mm thick sheets of low-carbon steel and 1.4 mm thick sheets of high-strength steel. The dog bone shape of the sample was employed according to the standard. In order to study the anisotropy of the material, three sets of samples were prepared along different directions. The moving speed of the chuck was set at 5 mm/min, which results in a strain rate of approximately 0.001 s^{-1} . The Young's modulus $E = 205 \text{ GPa}$ and Poisson's ratio $\nu = 0.33$ were obtained during the experiments. The r -value was calculated through the strain ratio of the thickness strain to the width strain. The detailed expression can be given as $r_\alpha = \varepsilon_w / \varepsilon_t$, where r_α is the obtained r -value along the α direction, ε_w is the width strain, and ε_t is the thickness strain. Figure 1 presents the uniaxial tension curves along 0, 45, and 90 degrees for both low-carbon steel (Figure 1a) and high-strength steel sheets (Figure 1b). According to these curves, the hardening and initial yield properties can be obtained through the power law function $(K(\varepsilon)^n)$. K and n are material constants. The detailed material parameters are listed in Tables 1 and 2 for the tested low-carbon steel and high-strength steel sheets, respectively.

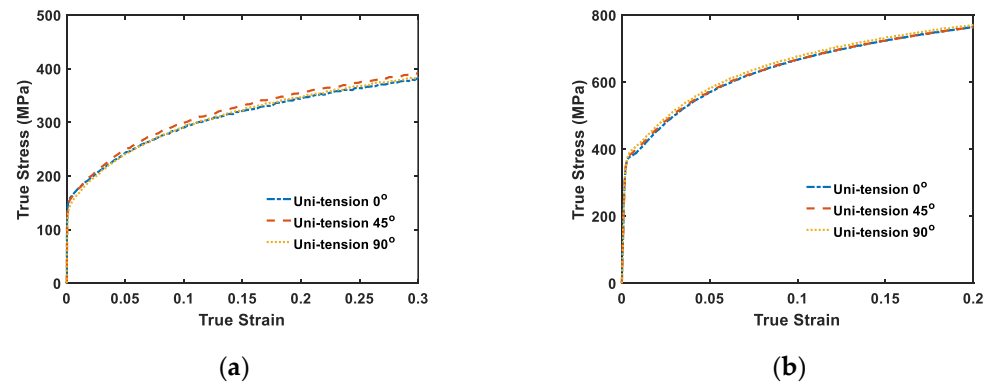


Figure 1. Uniaxial tension tests for (a) low-carbon steel sheet and (b) high-strength steel sheet.

Table 1. Material parameters along different directions (low-carbon steel).

Direction	r -Value	K (MPa)	n -Value	Yield Stress (MPa)
0	2.26	547.17	0.286	154
45	2.52	560.90	0.286	150
90	2.21	557.96	0.295	141

Table 2. Material parameters along different directions (high-strength steel).

Direction	r -Value	K (MPa)	n -Value	Yield Stress (MPa)
0	0.899	1120	0.212	341
45	0.946	1125	0.21	340
90	1.066	1128	0.209	331

2.2. The Forming Limit Tests

The experimental procedure for the Nakazima test was performed for the high-strength steel according to the ISO 12004-2:2008 [9]. The mini-Nakazima test was conducted, as shown in Figure 2a, for the low-carbon steel sheets. The test pieces recommended in the ISO 12004-2:2008 [14] were also used and modified in the experiments. The outer diameters of the samples were all 100 mm, but the remaining blank width was designed as 70 mm, 50 mm, 40 mm, and 30 mm, respectively. These four different specimen geometries were utilized to obtain different strain paths according to the finite element simulation results. A hemispherical punch with a 30 mm diameter was used. The specimen was clamped to the die with a blank holder force of 60 kN provided by the binder. A suitable number of draw beads were used to prevent slippage. The lubrication layer was placed between the punch and the specimen. According to the requirements of the standard, the lubricant system was composed of 0.06 mm thick polyethylene film and oil. The punch speed was set at 0.2 mm/s. At least three tests were repeated for each test piece geometry.

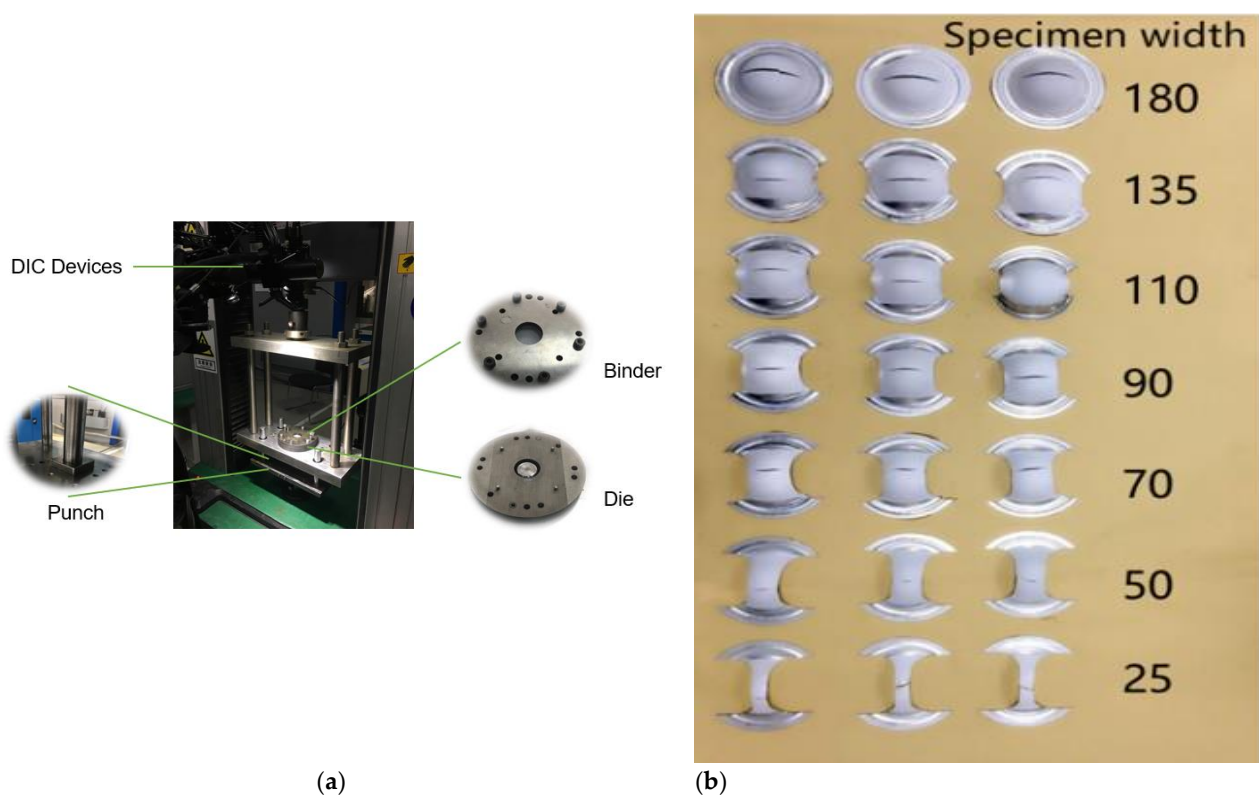


Figure 2. Experimental setup of the mini-Nakazima forming limit test and tested specimen (unit: mm): (a) experimental setup; (b) tested specimens.

The standard Nakazima test was conducted on 1.4 mm thick sheets of high-strength steel with the remaining specimen widths of 25 mm, 50 mm, 70 mm, 90 mm, 110 mm, 135 mm, and 180 mm (see Figure 2b). Similar lubrication was employed and static deformation was performed. The GOM Aramis optical strain measurement system was utilized. Before the measurement, a black and white random pattern was painted on the specimen surfaces for strain measurement. The image resolution, step size, and filter size were set as 0.051 mm/pixel, 5 pixels, and 3, respectively. Thus, the virtual strain gauge length (VSGL = resolution \times step size \times filter size) was 0.8 mm. The shooting frequency of the camera was set at 20 Hz in order to accurately record the relationship of strain over time [19–21].

2.3. Theoretical Models and Necking Interpretation

2.3.1. The Imperfection Method

Imperfection analysis assumes a pre-existing thickness defect denoted as a weak region in the form of a groove perpendicular to the principal strain direction in sheet metal. The loading direction and necking band orientation are along the X–Y and n–t coordinates, respectively. Strain localization occurs in the region of the groove when the strain increment in the weak band is 10~100 times greater than the strain increment in the normal region. The imperfection band rotates incrementally when the small strain increment is imposed, step by step, into the normal region. Typically, an initial band angle searching procedure from 0° to 90° at intervals of 1° is performed until the minimum localized necking strain is obtained. The detailed formulation of imperfection analysis refers to previous work [22,23].

The onset of localized necking in imperfection analysis can be understood as a bifurcation from a state of stable deformation. When the deformation concentrates in the weak band, a huge difference in the strain rate (or strain increments) can be found, as indicated in imperfection analysis, which manifests the beginning of an unstable deformation mode (or a bifurcation phenomenon in deformation). This bifurcation phenomenon satisfies a minimum energy principle for the plastic deformation of a sheet metal. Thus, stable plastic deformation, which is considered to be another deformation mode, will violate this principle and consume more energy to sustain.

2.3.2. The Non-Defect Method

Non-defect analysis under a continuum mechanics framework is also able to provide an alternative, but similar, understanding of the localized necking behavior of sheet metals. The strain concentrates in a certain band area that is eventually presented as a necking band with an initial crack in it. According to Stören and Rice [24], Zhu et al. [25], and Li et al. [26], the non-defect approach indicates that the condition of the necking onset will be satisfied if the non-zero solution of the difference in the rate of deformation (i.e., the bifurcation in deformation rate) exists. If only the zero solution of the difference in the rate of deformation is found, it then means that the deformation is still uniform between the inside and outside of the band. This implies an interesting material flow behavior in that the material close to the necking band will deform against the original trajectory to make the solution non-zero when necking occurs, which can be referred to as a bifurcation phenomenon.

2.4. Necking Evolution and Detection

Figure 3 shows the necking evolution of a 0.7 mm thick sheet of low-carbon steel with a remaining blank width of 40 mm. At the beginning of the experiment, a small area at the top of the hemispherical punch was in contact with the specimen. At this time, the strain was concentrated in the center of the specimen. As the experiment progressed, the area with the largest main strain gradually moved from the top to the side due to the limitation of the lubrication conditions. After 100 s of punch movement, two very obvious localized necking areas were formed. As shown in Figure 3, stage (d) was the last frame prior to fracture. This demonstrates that the strain showed localization during the forming limit experiments, and the necking groove was visible in the DIC-shaded surface image. Conversely, the sample almost no longer deformed outside the necking area. This process clearly shows that localized necking started with a narrow band and the material outside the band sustained no further plastic deformation after the observation of the necking band.

To detect localized necking, we first plotted the evolution curves for the major and minor strains versus time at different section points. A series of points were selected intensively in multiple cross-sections perpendicular to the direction of the necking band. These points were equidistant from the center of the necking zone to the outer region of the instability zone. In this scenario, three sections were studied, and five points were selected in each section. In the selected curves experiencing the bifurcation process, the maximum major strain value of the strain plateau of the selected material points was taken as the determined limit major strain; this was because this strain plateau indicates an obvious

strain bifurcation phenomenon during deformation, consistent with the theoretical and physical interpretations mentioned above. The moment corresponding to the achievement of maximum major strain was recorded and treated as the localized necking instant. The limit minor strain could then be easily determined since we already knew the corresponding necking instant, as well as its major strain.

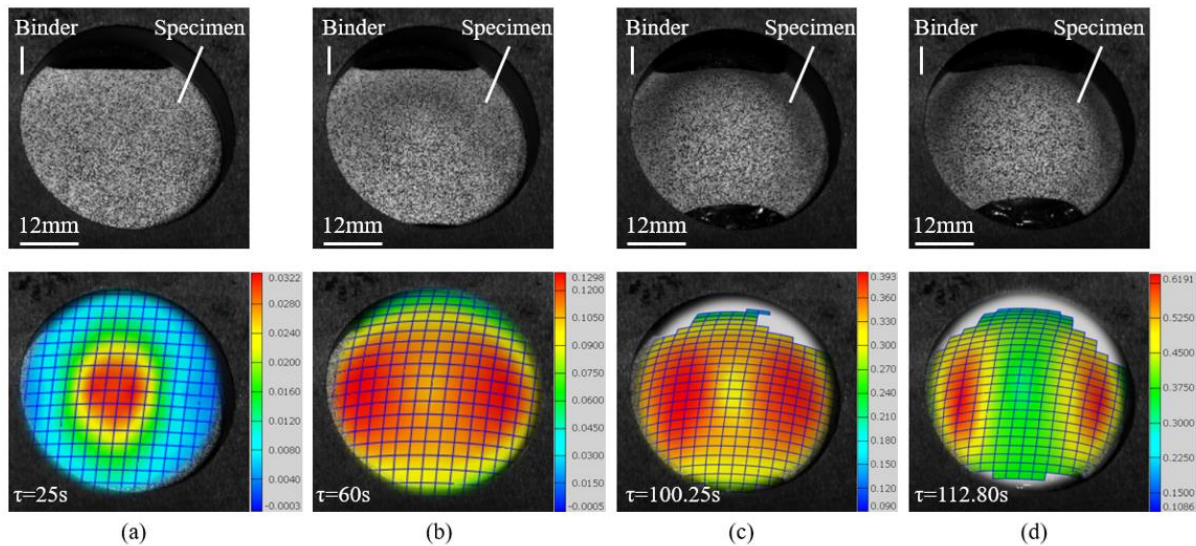


Figure 3. The necking formation in Nakajima tests (the legend denotes the true strain): (a) at the beginning of the experiment; (b) during the experiment; (c) after forming localized necking bands; and (d) prior to fracture.

The forming limit major and minor strain values for each section were obtained through the process illustrated above. The maximum limit major and minor strain for all sections (or the average of all obtained limit strains) can be used as the forming limit major and minor strains, respectively. The cross-section through the necking groove was created according to the DIC-shaded image. The results required for a detailed section view are almost insensitive to its alignment with the groove. The experimental results show little difference in the determined limit strain between the different sections (see the next section). This method is also insensitive to the geometry of the tooling, as both the Nakajima and Marciniak tests can be applicable since the detection process only considers the bifurcation in deformation.

3. Results and Discussion

3.1. The Bifurcation in Uniaxial Tension Test

This section discusses the high-strength steel test. Figure 4 shows the detailed material point selection on the uniaxial tension specimen. Five points were chosen across the strain localization area according to the strain concentration results of the DIC. Differences in both strain and strain rate evolution for material points 1~5 were expected since they were located inside and outside the necking band.

Figure 5a–c shows the experimental results for force, major strain rate, and major strain evolution during the uniaxial tension tests. Diffuse necking was determined through the maximum force principle. The instant of localized necking was also indicated in these figures, determined through the maximum strain rate. In Figure 5, the strain evolution shows the bifurcation phenomenon outside the necking band (see the strain plateau in Figure 5c) and continuous deformation behavior inside the band after localized necking. However, it shows that no such bifurcation phenomenon occurred during the diffuse necking in the selected material points (see Figure 5c).

Another interesting phenomenon indicates that the strain rate method determines localized necking based on the strain rate information of material point 2, which shows a

continuous deformation characteristic in its major strain evolution, as shown in Figure 5b,c. The strain rate method was proposed based on the first derivative calculation of major strain evolution. A convex curve is found in this calculation and its maximum value can be used to determine the instant of necking. However, its physical meaning is not completely understood. Another technology, named electronic speckle pattern interferometry (ESPI) [27], can be further utilized to help explain the physical meaning of DIC observations because this method appears to have better spatial resolution than the DIC for these types of measurements.

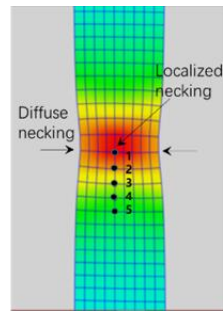


Figure 4. Illustration of selected material points for high-strength steel.

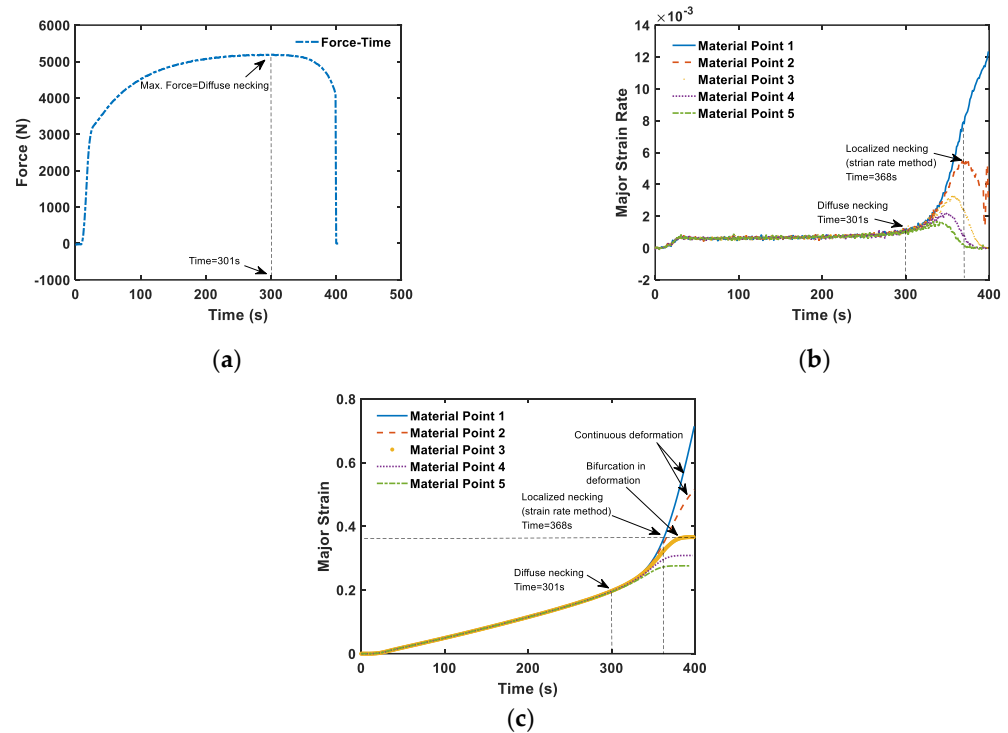


Figure 5. Force, major strain rate, and major strain evolution during uniaxial tension test of a high-strength steel sheet: (a) force–time evolution; (b) major strain rate evolution; (c) major strain evolution.

Furthermore, Figure 5 suggests that the major strain plateau can be used as an indicator to show the strain concentration in the necking band. In such a circumstance, the strain increment in the necking band becomes a hundred times bigger than the strain increment outside the band. This major strain plateau can be explained as a bifurcation in strain evolution from a state of continuous deformation (see material points 1 and 2 in Figure 5c). Thus, the major strain plateau can be utilized to indicate the formation of the limit strain, which shows a similar limit strain value as the value determined by the strain rate method (see Figure 5c).

To further compare the difference in strain rate for material points 1~5, we plotted the difference in major strain rates in Figure 6. The strain rate of material point 1 was treated as

the rate information inside the necking band, while other material points were assumed to be located outside the band. The non-zero value of the difference in major strain rates could be observed at the 335 s, which is earlier than the instant detected by the strain rate method (368 s). The results in Figure 6 show that the occurrence of the difference in strain rates inside and outside the thinning band provides a distinct localized necking strain, which underestimates the forming limits.

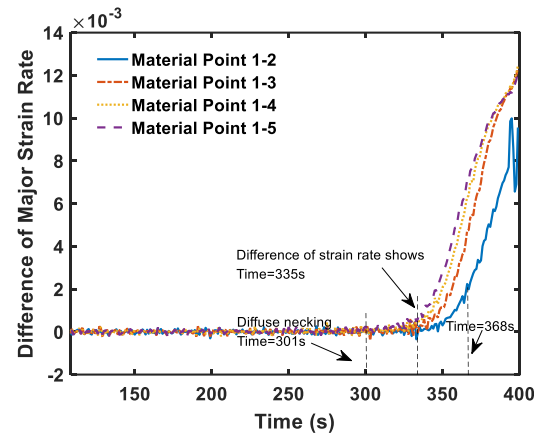


Figure 6. The difference in major strain rate of high-strength steel.

3.2. Localized Necking in Low-Carbon Steel

Figures 7–9 show the evolution of major strain and its rate in three independent tests based on the same specimen geometry of 40 mm width. The strain rate method was also employed to make a comparison. The instant of the localized necking onset was determined through the maximum major strain rate of the material, following which the relative strain inside the band was taken as the forming limit strain, which is similar to the methodology proposed by Martínez-Donaire et al. [14]. For each single test, three sections (referred to as a, b, and c) were analyzed to identify the differences from section to section. Five material points were selected; these were equidistant from the center of the necking zone to the outer region of the instability zone, as indicated in the section above.

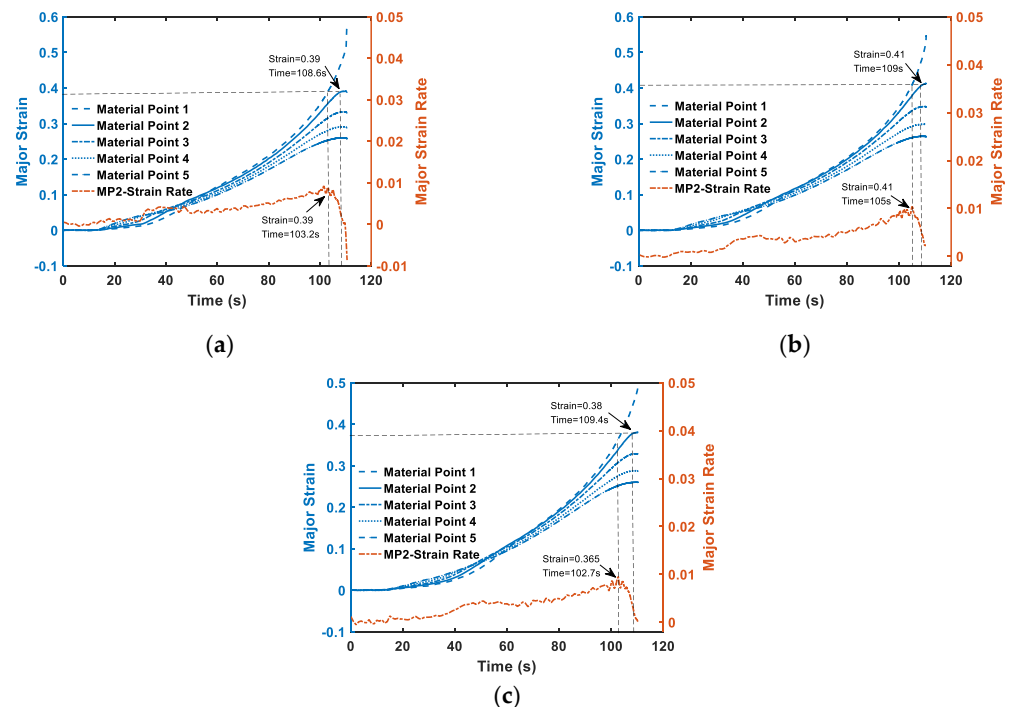


Figure 7. Major strain and strain rate evolution for the first test: (a) section a; (b) section b; (c) section c.

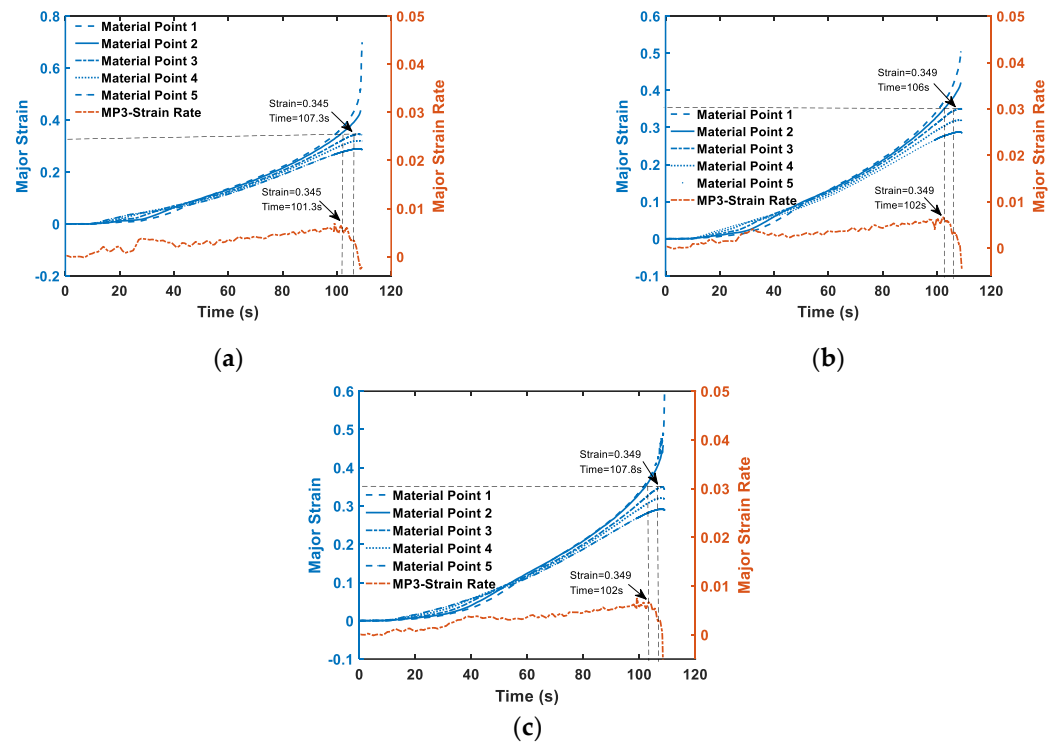


Figure 8. Major strain and strain rate evolution for the second test: (a) section a; (b) section b; (c) section c.

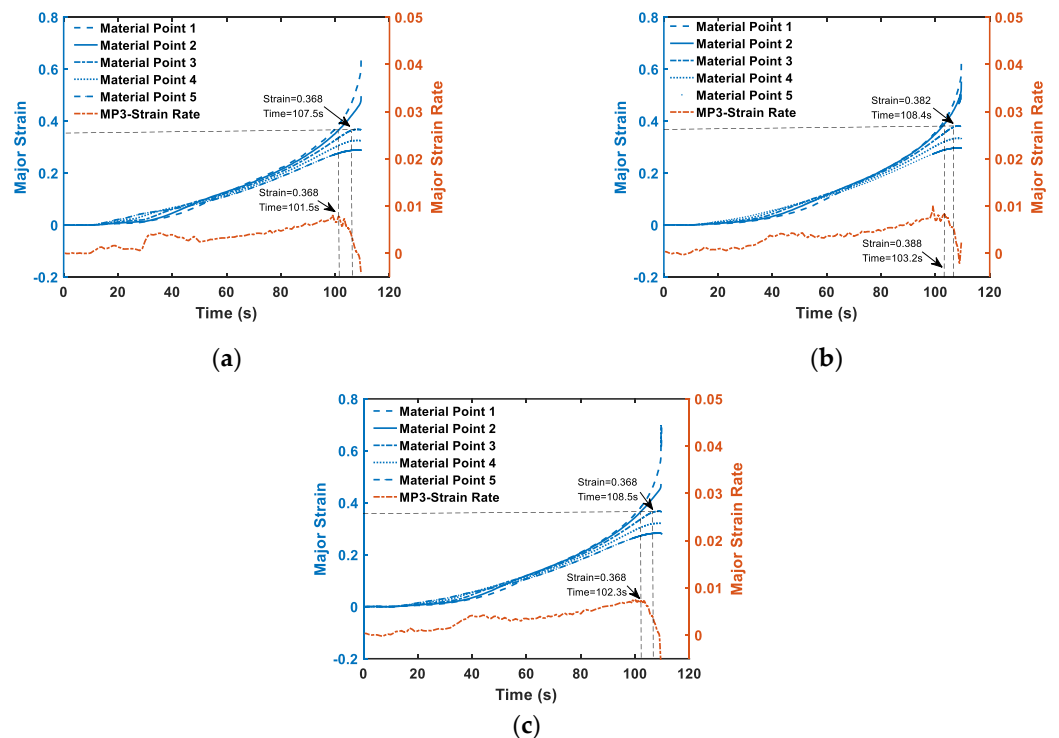


Figure 9. Major strain and strain rate evolution for the third test: (a) section a; (b) section b; (c) section c.

For the 40 mm wide specimens, all experimental major strain results show an obvious strain plateau, which can be taken as a detector of the strain concentration in the weak band. Figures 7–9 show that the bifurcation (or the major strain plateau) in the major strain evolution indicates almost the same forming limit major strain as the strain rate method. However, the instant of the localized necking onset was different, as also shown in these figures. One noteworthy point is that as the strain rate signals were obtained through the

major strain derivative, noisy data were present and required mathematical smoothing treatment before limit strain detection. For the proposed method, only a strain signal was utilized, and no further mathematical treatment was necessary. As can be seen in Figures 7–9, different sections of the same tests provided similar limit major strains, which serves as evidence of the stability of the proposed method in terms of its cross-section selection. These nine different plots also act as direct experimental evidence demonstrating that the proposed method provides a similar necking limit strain as the strain rate method.

Table 3 summarizes the determined forming limit major strains and necking instants for the three independent tests using the proposed method. The difference in final results is not significant. This suggests the proposed necking detection approach can be used as a stable method to extract experimental results.

Table 3. Summary of the limit major strain of low-carbon steel sheet with 40 mm width specimen of three independent tests.

Specimen	Section a		Section b		Section c	
	Limit Strain	Necking Time	Limit Strain	Necking Time	Limit Strain	Necking Time
1	0.39	108.6 s	0.41	109 s	0.38	109.4 s
2	0.345	107.3 s	0.349	106 s	0.349	107.8 s
3	0.368	107.5 s	0.382	108.4 s	0.368	108.5 s

For other linear path experiments on low-carbon steel, in Figures 10 and 11, we present the test results for 70 mm wide and 30 mm wide specimens. The major strain evolution results for two independent tests are shown separately in (a) and (b). Clearly, the strain plateau could be directly observed at the end of its strain evolution, and the final forming limit strains were almost the same. However, in these tests, the strain rate method could barely distinguish the maximum rate value before the drop, for which a more advanced smoothing method should be utilized to achieve satisfactory results. Fortunately, the strain rate method was not the focus of this study, although it serves as a comparison against the new proposed method.

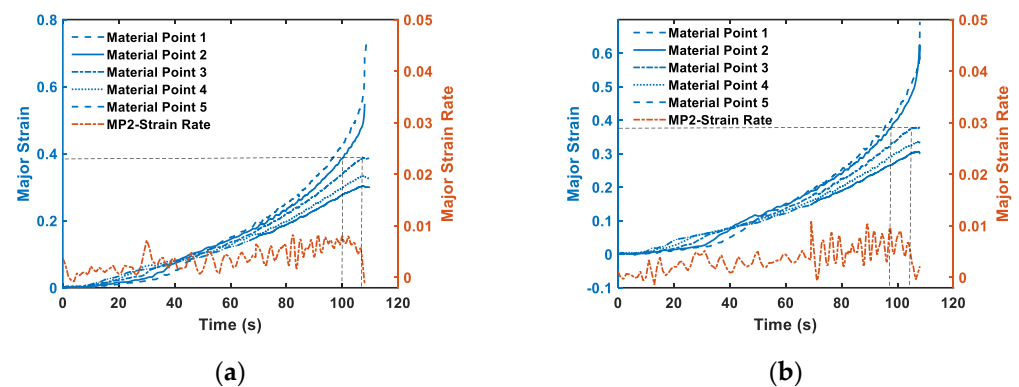


Figure 10. Major strain and strain rate evolution for two independent tests on a 70 mm wide specimen: (a) the first test; (b) the second test.

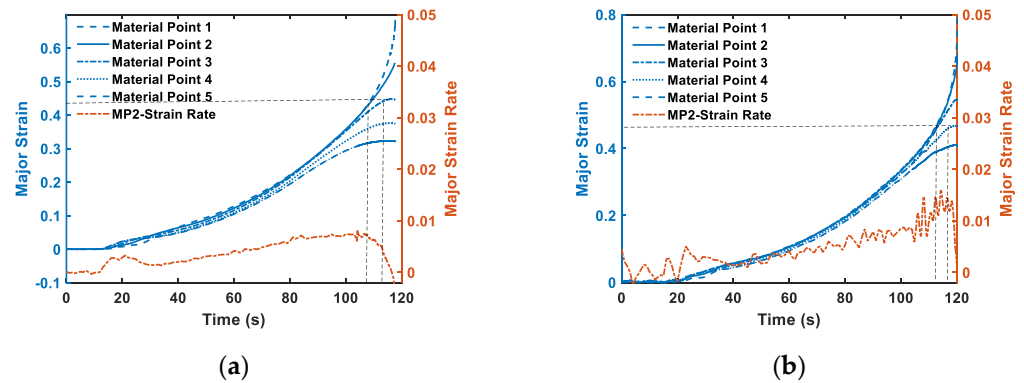


Figure 11. The major strain and strain rate evolution for two independent tests on a 30 mm wide specimen: (a) the first test; (b) the second test.

3.3. Localized Necking in DP Steel Sheets

Standard Nakajima tests were performed using DP steel sheets, where seven different specimens were utilized to determine necking strain and further verify the stability of the proposed method. Specimens with widths of 25 mm (uniaxial tension), 110 mm (plane strain tension), and 180 mm (balanced biaxial tension) were taken as demonstrators in this section. Figures 12–14 present the detailed major strain and strain rate evolutions for two independent tests. For the uniaxial tension mode in Figure 12, the strain rate method produces a convex curve, where the maximum strain rate indicates the forming limit strain. The results of plane strain deformation mode in Figure 13 also show satisfactory agreement for the two independent tests, where a similar necking strain can be obtained through the new method. However, the experimental results for the balanced biaxial tension mode in Figure 14 show no strain plateau, and the strain evolution of all selected material points monotonously increased without bifurcation phenomenon. The strain rate method offers a sudden drop in major strain rate evolution, but its physical meaning is not explicit.

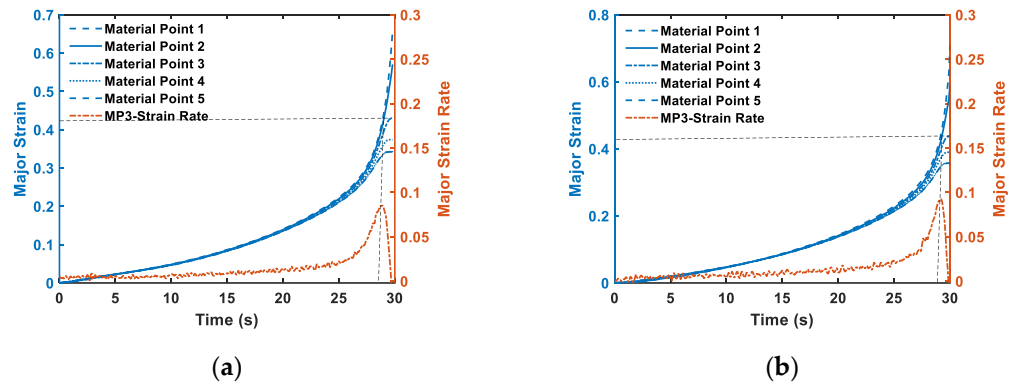


Figure 12. Major strain and strain rate evolution for two independent tests on a 25 mm wide specimen: (a) the first test; (b) the second test.

The thickness of several material points on three cross-sections perpendicular to the crack direction was measured to reflect the final necking condition, as shown in Figure 15a. The balanced biaxial tension specimen shows a small difference (approximately 7% difference) in thickness distribution from the crack edge to the outer region of the instability zone. For uniaxial and plane strain tension modes, thinning that exceeds 0.15 mm can be observed in Figure 15a, which suggests a severe necking procedure before the fracture occurred. An enlarged crack edge can be observed in the balanced biaxial tension specimen presented in Figure 15b. Almost no thinning phenomenon can be seen in the crack edge, and the fracture surface aligns at approximately 45° . The obtained information suggests that failure under the balanced biaxial tension mode of the high-strength steel was caused by a direct fracture rather than localized necking.

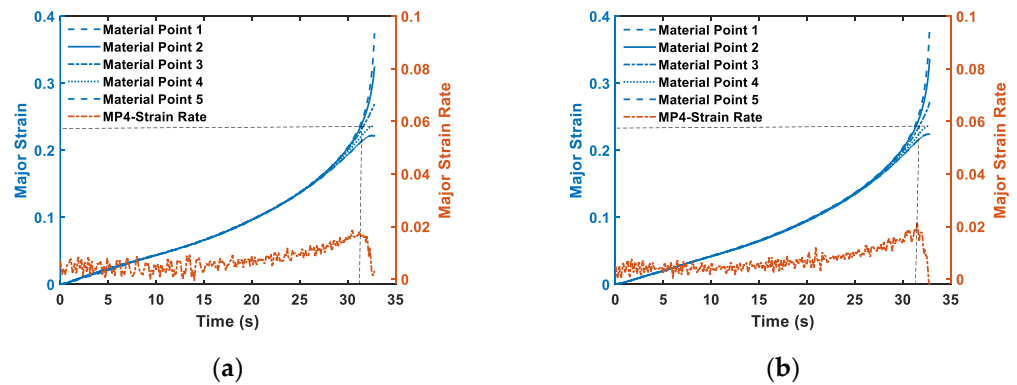


Figure 13. Major strain and strain rate evolution for two independent tests on a 110 mm wide specimen: (a) the first test; (b) the second test.

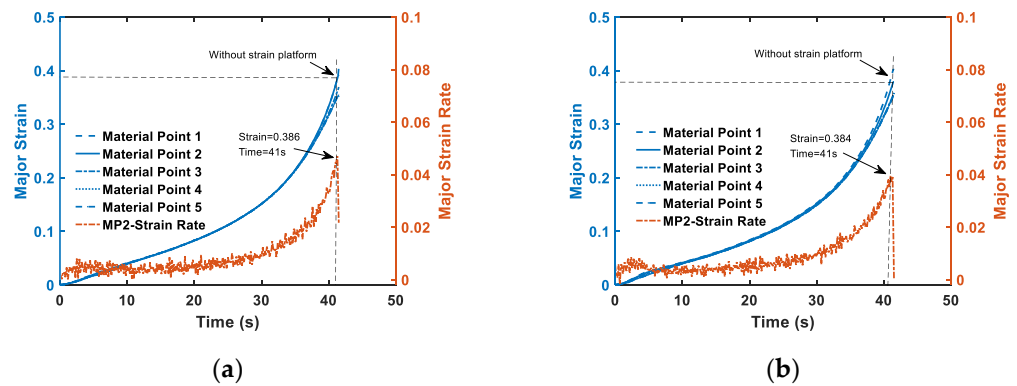


Figure 14. Major strain and strain rate evolution for two independent tests on a 180 mm wide specimen: (a) the first test; (b) the second test.

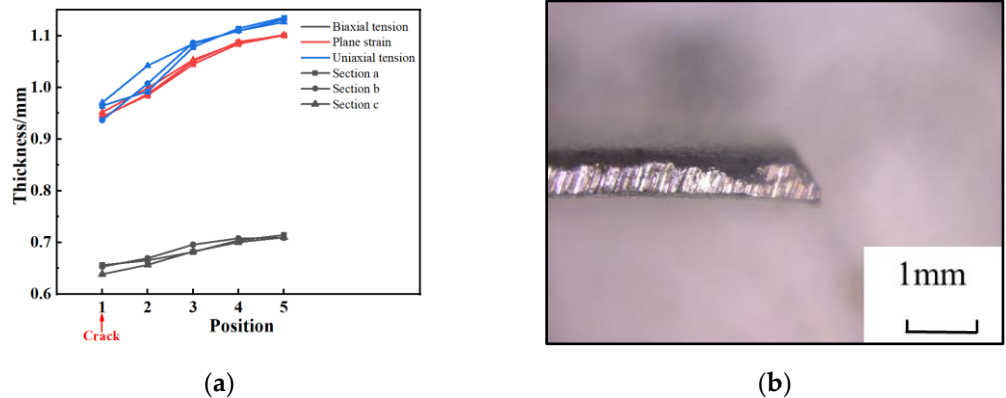


Figure 15. The thickness distribution of different tests and the observation of the crack edge of balanced biaxial tension specimen: (a) thickness distribution of different section cuts and locations; (b) the observation of the crack edge.

3.4. Forming Limit Diagram

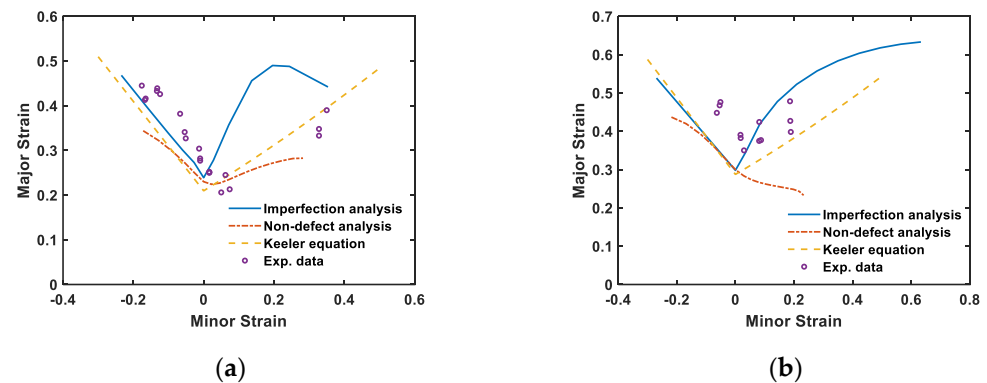
All obtained experimental forming limit strains for the high-strength steel sheet are summarized in Table 4. The final results from the three independent tests for each test piece geometry are all presented. The forming limit strains of low-carbon steel are further presented in Table 5. Keeler’s equation [2] was also utilized as a compensation for the experiments (see Figure 16a,b). Non-defect and imperfection predictions were both employed to predict the forming limits and compared with experimental data, as shown in Figure 16.

Table 4. Summary of the forming limit strain of high-strength steel sheet.

Specimen Width (Unit: mm)	Test	Major Strain	Minor Strain
25	1	0.445	−0.176
	2	0.416	−0.165
	3	0.413	−0.167
50	1	0.426	−0.124
	2	0.433	−0.133
	3	0.439	−0.132
70	1	0.382	−0.067
	2	0.327	−0.051
	3	0.341	−0.054
90	1	0.304	−0.013
	2	0.282	−0.010
	3	0.277	−0.010
110	1	0.250	0.016
	2	0.252	0.016
	3	0.251	0.016
135	1	0.206	0.050
	2	0.213	0.074
	3	0.245	0.062
180 (strain rate method)	1	0.348	0.328
	2	0.386	0.350
	3	0.333	0.328

Table 5. Summary of the forming limit strain of low-carbon steel sheet.

Specimen Width (Unit: mm)	Test	Major Strain	Minor Strain
30	1	0.448	−0.064
	2	0.476	−0.051
	3	0.468	−0.054
40	1	0.391	0.017
	2	0.35	0.029
	3	0.382	0.018
50	1	0.375	0.081
	2	0.377	0.087
	3	0.424	0.081
70	1	0.478	0.186
	2	0.398	0.189
	3	0.427	0.187

**Figure 16.** Comparison of the experimental data and predicted results using non-defect analysis, imperfection analysis, and Keeler's equation: (a) high-strength steel; (b) low-carbon steel.

In non-defect analysis, the r -value was directly used to determine the coefficients of the yield function [26]. Another strategy would be to use the yield stress to determine

the anisotropic coefficients; however, this would cause more deviation since the forming limit prediction was largely affected by the plastic flow direction (or r -value) when necking occurred. When imperfection analysis was performed, the non-associated flow rule was adopted through Hill's 48 function [23], where the yield stress and r -values were all considered in constitutive model. This would be expected to be a more reasonable predictor with limited parameters. The anisotropic material parameters were determined for both yield surface and plastic potential and are further summarized in Tables 6 and 7. $F_y \sim N_y$ were anisotropic yield coefficients determined by yield stresses, while $F_p \sim N_p$ were plastic flow coefficients determined by r -values.

Table 6. Summary of the anisotropic coefficients of low-carbon steel.

Material	F_y	G_y	H_y	N_y	F_p	G_p	H_p	N_p
Low-carbon steel	0.64	0.45	0.55	1.56	0.31	0.31	0.69	1.87

Table 7. Summary of the anisotropic coefficients of high-strength steel.

Material	F_y	G_y	H_y	N_y	F_p	G_p	H_p	N_p
High-strength steel	0.55	0.48	0.52	1.5	0.44	0.53	0.47	1.4

Figure 16a,b show a comparison between the imperfection analysis prediction and the experimental data. On the left-hand side of the forming limit curve, all predictions produced a consistent and reliable performance. The deviation between the prediction and the experimental data is not significant. However, at the right-hand side, the non-defect analysis largely underestimates the forming limit curve in scenarios with low-carbon steel sheets, but it presents broadly good prediction when it is compared with the data for high-strength steel sheets. This phenomenon results from the more complicated anisotropic behavior of low-carbon steel, which cannot be accurately captured by Hill's 48 function. However, to consider a more advanced yield function (high order or more parameters) in non-defect analysis, a cumbersome deduction is required, which is not the focus of this study. It seems that the non-associated flow rule model with Hill's 48 function based on imperfection analysis can also be used to reliably estimate the forming limit results. This comparison helps to verify the quality of the obtained forming limit strains, as well as the proposed necking deterministic approach.

4. Conclusions

In this paper, a new deterministic approach to localized necking for experimental forming limit strains, based on the physical understanding of the necking process, was proposed. Two different sheet-metal steels were utilized through the Nakazima and mini-Nakazima tests to verify the proposed method. Imperfection and non-defect analysis were performed, utilizing the non-associated and associated flow rules by using the baseline material test data, while comparisons between the predictions and experiments were performed. Several conclusions are provided as follows:

1. The proposed localized necking deterministic approach can reliably capture the forming limits, and the obtained strain limit is similar to the results determined by the strain rate method. This method is based on the bifurcation phenomenon (or the strain plateau) of sheet metals without the derivative calculation of strain evolution, which implies a localized deformation in a narrow band, while the deformation remains homogeneous elsewhere to form the strain plateau during localized necking.
2. The proposed method shows a good agreement on the left-hand side when compared to a theoretical prediction. For low-carbon steel sheets, the new method shows satisfactory agreement between the imperfection prediction, Keeler's equation, and the experiments. For high-strength steel sheets, more tests are still necessary to achieve a full comparison.

-
-
3. The failure mode of the high-strength steel sheets tested in this study under balanced biaxial tension shows a very complex mechanism. Based on the thickness measurement, as well as crack edge observation, it is suggested that a direct fracture occurred before localized necking.

Author Contributions: J.H.: conceptualization, methodology, formal analysis, software, writing-original draft, investigation, analysis; Y.F.: experimental validation, analysis. All authors have read and agreed to the published version of the manuscript.

Funding: This study was supported by Ji He's academic grants as follows: National Natural Science Foundation of China (grant no.51975364) and the State Key Laboratory of Mechanical Systems and Vibration (grant no. MSVZD202207).

Data Availability Statement: The processed data generated and analyzed during the current study are available from the corresponding author on reasonable request.

Acknowledgments: Financial support from the National Natural Science Foundation of China (grant no. 51975364 and 51790170) and the State Key Laboratory of Mechanical Systems and Vibration (grant no. MSVZD202207) are gratefully acknowledged.

Conflicts of Interest: The authors declare that they have no known competing financial interest or personal relationships that could have appeared to influence the work reported in this paper.

References

1. Hill, R. On Discontinuous Plastic States with Special Reference to Localized Necking in Thin Sheets. *J. Mech. Phys. Solids* **1952**, *1*, 19–30. [\[CrossRef\]](#)
2. Keeler, S. *Determination of Forming Limits in Automotive Stampings*; SAE Technical Paper, No. 650535; SAE International: Warrendale, PA, USA, 1965. [\[CrossRef\]](#)
3. Goodwin, G.M. *Application of Strain Analysis on Sheet Metal Forming Problems in the Press Shop*; SAE Technical Paper; No. 680093; SAE International: Warrendale, PA, USA, 1968.
4. He, J.; Han, G.F.; Feng, Y.S. Phase transformation and plastic behavior of QP steel sheets: Transformation kinetics-informed modeling and forming limit prediction. *Thin Walled Struct.* **2022**, *173*, 108977. [\[CrossRef\]](#)
5. Han, G.F.; He, J.; Li, S.H. Simple shear deformation of sheet metals: Finite strain perturbation analysis and high-resolution quasi-in-situ strain measurement. *Int. J. Plasticity* **2022**, *150*, 103194. [\[CrossRef\]](#)
6. He, J.; Han, G.F.; Li, S.H.; Zou, D.Q. To correlate the phase transformation and mechanical behavior of QP steel sheets. *Int. J. Mech. Sci.* **2019**, *152*, 198–210. [\[CrossRef\]](#)
7. He, J.; Xia, Z.C.; Zhu, X.H.; Zeng, D.; Li, S.H. Sheet Metal Forming Limits under Stretch-Bending with Anisotropic Hardening. *Int. J. Mech. Sci.* **2013**, *75*, 244–256. [\[CrossRef\]](#)
8. He, J.; Zeng, D.; Zhu, X.H.; Xia, Z.C.; Li, S.H. Effect of Nonlinear Strain Paths on Forming Limits under Isotropic and Anisotropic Hardening. *Int. J. Solids Struct.* **2014**, *51*, 402–415. [\[CrossRef\]](#)
9. *ISO-FDIS 12004-2-2008*; Metallic Materials-Sheet and Strip-Determination of Forming Limit Curves. International Organization for Standardization: Geneva, Switzerland, 2008.
10. Marciniak, Z.; Kuczynski, K. Limit Strains in the Processes of Stretch-Forming Sheet Metal. *Int. J. Mech. Sci.* **1967**, *9*, 609–612. [\[CrossRef\]](#)
11. Huang, G.; Sriram, S.; Yan, B. Digital image correlation technique and its application in forming limit curve determination. In Proceedings of the IDDRG 2008 International Conference, Olofstrom, Sweden, 16 June 2018; pp. 153–162.
12. Merklein, M.; Kuppert, A.; Geiger, M. Time dependent determination of forming limit diagrams. *CIRP Ann. Manuf. Technol.* **2010**, *59*, 295–298. [\[CrossRef\]](#)
13. Hotz, W.; Merklein, M.; Kuppert, A.; Friebe, H.; Klein, M. Time dependent FLC determination-Comparison of different algorithms to detect the onset of unstable necking before fracture. *Key Eng. Mater.* **2013**, *549*, 397–404. [\[CrossRef\]](#)
14. Martínez-Donaire, A.J.; García-Lomas, F.J.; Vallellano, C. New approaches to detect the onset of localized necking in sheets under through-thickness strain gradients. *Mater. Des.* **2014**, *57*, 135–145. [\[CrossRef\]](#)
15. Min, J.; Stoughton, T.B.; Carsley, J.E.; Lin, J. Comparison of DIC methods of determining forming limit strains. *Procedia Manuf.* **2017**, *7*, 668–674. [\[CrossRef\]](#)
16. Wang, K.; Carsley, J.E.; He, B.; Li, J.; Zhang, L. Measuring forming limit strains with digital image correlation analysis. *J. Mat. Process Tech.* **2014**, *214*, 1120–1130. [\[CrossRef\]](#)
17. Di Cecco, S.; Butcher, C.; Worswick, M.; Chu, E.; Boettcher, E.; Shi, C. Determination of forming limit diagrams of AA6013-T6 aluminum alloy sheet using a time and position dependent localized necking criterion. *IOP Conf. Ser. Mater. Sci. Eng.* **2016**, *159*, 012009. [\[CrossRef\]](#)

18. Min, J.; Stoughton, T.B.; Carsley, J.E.; Lin, J. A method of detecting the onset of localized necking based on surface geometry measurement. *Exp. Mech.* **2016**, *57*, 521–535. [[CrossRef](#)]
19. Gu, B.; He, J.; Li, S.H.; Lin, Z.Q. Anisotropic fracture modeling of sheet metals: From in-plane to out-of-plane. *Int. J. Solids Struct.* **2019**, *182–183*, 112–140. [[CrossRef](#)]
20. Guo, C.; He, J.; Su, Y.H.; Li, S.H. Thermo-stamping co-curing process for CFRP/steel hybrid sheets and its interface strength improvement. *Compos. Struct.* **2020**, *241*, 112108. [[CrossRef](#)]
21. Guo, C.; He, J. Multi-scale concurrent analysis for bio-inspired helicoidal CFRP laminates and experimental investigation. *Compos. Struct.* **2022**, *296*, 115886. [[CrossRef](#)]
22. He, J.; Li, Y.F.; Gu, B.; Li, S. Effects of reverse loading on forming limit predictions with distortional anisotropic hardening under associated and non-associated flow rules. *Int. J. Mech. Sci.* **2019**, *156*, 446–461. [[CrossRef](#)]
23. He, J.; Han, G.; Guo, C. Non-associated anisotropic plasticity of metal sheets based on the distortional concept. *Thin Walled Struct.* **2021**, *161*, 107523. [[CrossRef](#)]
24. Stören, S.; Rice, J. Localized Necking in Thin Sheets. *J. Mech. Phys. Solids* **1975**, *23*, 421–441. [[CrossRef](#)]
25. Zhu, X.H.; Weinmann, K.; Chandra, A. A Unified Bifurcation Analysis of Sheet Metal Forming Limits. *ASME J. Eng. Mater. Technol.* **2001**, *123*, 329–333. [[CrossRef](#)]
26. Li, S.; He, J.; Cedric Xia, Z.; Zeng, D.; Hou, B. Bifurcation Analysis of Forming Limits for an Orthotropic Sheet Metal. *ASME J. Manuf. Sci. Eng.* **2014**, *136*, 051005. [[CrossRef](#)]
27. Petit, J.; Montay, G.; François, M. Strain rate measurements by speckle interferometry for necking investigation in stainless steel. *Int. J. Solids Struct.* **2014**, *51*, 540–550. [[CrossRef](#)]

Disclaimer/Publisher’s Note: The statements, opinions and data contained in all publications are solely those of the individual author(s) and contributor(s) and not of MDPI and/or the editor(s). MDPI and/or the editor(s) disclaim responsibility for any injury to people or property resulting from any ideas, methods, instructions or products referred to in the content.